Supplementary material for Hansen et al., A simulation study on proton CT stopping power accuracy using dual energy CT scans as benchmark, Acta Oncol, 2015; 54: 1638–1642.

Appendix

Material and methods

Calculating the range of protons in proton therapy is done via the stopping power, defined as the energy lost per unit distance. For a given medium, this can be calculated theoretically via the Bethe equation [1]

$$\frac{dE}{dx} = \frac{4\rho_e \pi e^4}{m_e v^2}\frac{1}{u} z^2 \left[\ln\frac{2 m_e v^2}{I} + \ln\left[\frac{1}{1-\beta^2} - \beta^2\right]\right] \quad (1)$$

where ρ_e is the electron density, e is the electron charge, m_e the electron mass and u the atomic mass unit, v the velocity and z the charge of the projectile. I is the mean excitation energy of the medium and $\beta = \frac{v}{c}$.

For compounds, the mean excitation energy is typically calculated via the Bragg additivity rule [2]. This is generally reasonably accurate, but for some low-Z materials it can show deviations of up to 50% [3].

In order to estimate the uncertainty associated with calculated stopping power, the data from [4] was used in this work.

Hünemohr *et al* [4] measured stopping power of their phantom inserts experimentally. This was done by measuring the range of a 200MeV/u ^{12}C ion beam in a water column after penetrating one of the inserts. They also reported the stoichiometric composition of the phantom compounds. The data from their work can thus be used to estimate the discrepancy between calculated and measured stopping power. By comparing the theoretical stopping power with the measured, and taking the experimental precision into account, the uncertainty of using theoretical values can be calculated through

$$\sigma_{theory} = \sqrt{\sigma_{diff}^2 - \sigma_{exp}^2} \quad (2)$$

where σ_{exp} is the experimental uncertainty and σ_{diff} is the root mean square of the difference between the measured and calculated stopping power.

Stopping power estimation from SECT

The Hounsfield units (HU) obtained in x-ray CT are a transformation of the attenuation coefficients of the materials scanned. This can be calculated by

$$\mu(E) = \rho N_A \sum_i (i=1)^N [w_i/A_i (K_{ph}(E) Z_i^n + K_{coh}(E) Z_i^m + K_{KN}(E)] \quad 3)$$

where K_{ph}, K_{coh} and K_{KN} are the energy dependent photo-electric, Klein-Nishina, and coherent scattering coefficients respectively and Z_i is the atomic number of the ith element with relative contribution w_i to the mass of the material made of N elements and with mass density ρ . m and n are constants and are typically given the values 2.86, and 4.62 respectively [5].

Due to the large dependence on the atomic number, it is clear that no direct relation can be established between x-ray attenuation units and stopping power.

This is further complicated by the fact that the attenuation measured in x-ray CT is a weighted average from a spectrum of energies, rather than a mono-energetic contribution. The simplest approach relies on a piece-wise linear relation based on measurements of HU and stopping power of a phantom. The problem with this approach is that the stoichiometric composition of the phantom materials is rarely a good substitute for human tissue. Instead, state of the art is the stoichiometric method [6]. For a photon spectrum, the HU are

$$HU = 1000 \cdot \frac{\rho}{\rho_{H2O}} \frac{\sum_{i=1}^{N} \left(\frac{w_i}{A_i}\right)(Z_i + Z_i^{2.86} + Z_i^{4.62} k_2)}{\left(\frac{w_H}{A_H}\right)(1 + k_1 + k_2) + \left(\frac{w_O}{A_O}\right)(8 + 8^{2.86} k_1 + 8^{4.62} k_2)} \quad 4)$$

where $k_1 = \frac{\overline{K^{coh}}}{\overline{K^{KN}}}$ and $k_2 = \frac{\overline{K^{ph}}}{\overline{K^{KN}}}$ [7]. Here w_H, A_H, w_O and A_O indicate the fraction and atomic weight of hydrogen and oxygen in water. $\bar{X}$ indicates the spectrum averaged quantity, indicating that k_1 and k_2 are dependent on the x-ray spectrum and therefore the specific CT scanner.

In the stoichiometric method, a phantom with inserts which need not be human tissue equivalent, but with known ρ , ρ_e and Z_i is scanned. k_1 and k_2 are then found by fitting to equation 4. Theoretical HUs and stopping power relative to water are calculated for a number of reference tissue compositions taken from [8] using equation

4. A piece-wise linear relation, consisting of 4 segments is then fitted to this. For tabulated human tissue compositions [8] , this yields estimates accurate within 3.5% for 95% of all patients [9].

Stopping power estimation from DECT

In DECT, attenuation coefficients for two x-ray spectra are obtained, either by scanning the patient with two different energies or by employing detectors with differential energy response. This allows for the calculation of the electron density and mean excitation potential needed to calculate stopping power from equation 1

Electron density

Saito [10] introduced the dual energy subtracted quantity ΔHU

$$\Delta HU \equiv (1+\alpha)HU(H) - \alpha HU(L) \qquad 5)$$

where $HU(H)$ and $HU(L)$ are the Hounsfield values obtained from the high and low energy spectra respectively and α is a scanner specific weighting factor. A linear relation between this quantity and electron density was then established

$$\rho_e = \frac{a_\rho \Delta HU}{1000} + b_\rho \qquad 6)$$

a_ρ and b_ρ can then be obtained via a calibration, while α is chosen to minimize the residuals in the calibration scan.

The method was subsequently shown to have an accuracy of better than 1.0% for most materials [11].

I-value

Equation 3 is valid for a single photon energy only, whereas the HUs measured in a CT scanner are the result of a full photon spectrum.

In [12], it was suggested that the HUs could be approximated for human tissues by

$$HU(S) \approx 1000 \cdot \rho\left(A(S) + B(S)Z_{eff}^{n-1} + C(S)Z_{eff}^{m-1}\right) - 1000 \qquad 7)$$

where ρ is the material density. A(S), B(S) and C(S) are energy response weighted averages of the K factors from equation 3 and are dependent on the x-ray spectrum S. Z_{eff} is the weighted average atomic number of the material in a given CT voxel.

For a DECT scan, the ratio between the scans is then given by

$$\frac{\frac{HU(H)+1000}{1000}}{\frac{HU(L)+1000}{1000}} \approx \frac{A(H)+B(H)Z_{eff}^{n-1}+C(H)Z_{eff}^{m-1}}{A(L)+B(L)Z_{eff}^{n-1}+C(L)Z_{eff}^{m-1}} \quad 8)$$

Yang *et al* [13] established an empirical correlation for human tissues between the effective atomic number and the logarithm of the *I*-value through a piece-wise linear relation

$$\ln(I) = a_I Z_{eff} + b_I$$

where a_I and b_I are model parameters. In this work, we use two sections (($Z_{eff} < 8.2$) and ($Z_{eff} > 9$)) fitted to the tissues from [8][8]. Only one human tissue material (thyroid) is present in the remaining region, for which a constant value is then used.

The relevant SECT and DECT calibration functions are presented in Fig. A1.

Proton CT based stopping power estimation

In proton CT, high energy protons are shot through the patient and their kinetic energy recorded on the other side. Based on the continuous slowing down approximation (CSDA), the water-equivalent path-length (WEPL) can then be calculated for each individual proton via the equation

$$WEPL(E_{in}, E_{out}) = \int_{E_{in}}^{E_{out}} \left(\frac{dE}{dx_{water}}\right)^{-1} dE. \quad 9)$$

Here E_{in} and E_{out} are the kinetic energies of the proton before and after penetrating the object.

Transforming energy loss into WEPL makes the reconstruction problem linear, similar to what the log-transform does for standard x-ray CT. The water-equivalent stopping power (WESP) can then be reconstructed by iterative or direct methods. In this work, we used an iterative reconstruction method previously described [14] which solves the minimization problem

$$\min_{x} \|Ax - b\| \quad (10)$$

where **b** is a vector containing the WEPLs for the individual protons and **x** is the image to be reconstructed.

A is the linear system transform, performing the line integral of each proton through the image.

Here, the proton trajectories were modelled via cubic splines to account for scattering, as suggested in [15]. Note that the reconstruction is based on the assumption that the ratio between the stopping power of water and the stopping power of other materials is constant with energy.

This would be accurate if all materials had the same *I*-value. Schulte *et al* [16] state that for adipose tissue and compact bone this results in an error of up to 2%, while for muscle the error is virtually zero. However, the majority of this error happens close to the proton end range, and before the last 2.5cm of the proton range the error is less than 0.5%.

The reconstructions were performed on a Geforce GTX Titan BLACK GPU (NVIDIA, Santa Clara, USA) using the Gadgetron framework [17].

Monte Carlo Simulation

Digital replicas of the Gammex and CIRS phantoms, described in the main manuscript, were made in the Monte Carlo code Geant4 [18]. The EM standard 3 physics list was used for all atomic interactions, including range straggling and multiple scattering. The hadron inelastic QBBC physics list was used for nuclear fragmentation. Production of secondary electrons, positrons, and photons was disabled to increase calculation speed, as these would have no impact on the scan. Each phantom was scanned using a uniform field of 250MeV protons at a CT equivalent dose index (CTEDI) [14] of 10 mSv.

An energy spread of =0.5MeV was used, which is well within what can be achieved clinically [19]. For the purpose of a comparison, a realistic modelling of a proton CT scanner is important. This work is based on the setups and detectors used in [20] and [21] (see Figure A2).

During the simulation, the detectors had 100% efficiency and perfect accuracy. Noise, corresponding to what can be achieved with real detectors, was then added post-simulation. To register position and direction of the protons, we assumed that four silicon strip detectors, each 200μm thick, were placed pair-wise on each side of the phantom.

Following [21], the distance between the detectors in each pair was 5.0cm. $_{xy=}$200μm was added to the data from all four silicon detectors, based on the pitch reported in the literature [20, 21]. We assumed that a YAG:Ce

calorimeter was placed after the last position detector. This was modelled after the PRIMA calorimeter, and detector response and noise were done following [20].

Based on a fit of the experimental characterization, noise corresponding to

$$\sigma_E(E) = \max\left(3\% \cdot E, \frac{24.15MeV^2}{E} + 1.76MeV\right) \quad 11)$$

was added to the calorimeter data post simulation.

References

[1] Bethe H. Zur Theorie des Durchgangs schneller Korpuskularstrahlen durch Materie. Ann Phys 1930;397:325-400.

[2] ICRU. Stopping power and ranges for protons and alpha particles. 1993.

[3] Thwaites DI. Bragg Rule of Stopping Power Additivity - a Compilation and Summary of Results. Radiat Res 1983;95:495-518.

[4] Hunemohr N, Krauss B, Tremmel C, Ackermann B, Jakel O, Greilich S. Experimental verification of ion stopping power prediction from dual energy CT data in tissue surrogates. Phys Med Biol 2014;59:83-96.

[5] Rutherford RA, Pullan BR, Isherwood I. Measurement of Effective Atomic Number and Electron-Density Using an Emi Scanner. Neuroradiology 1976;11:15-21.

[6] Schneider U, Pedroni E, Lomax A. The calibration of CT Hounsfield units for radiotherapy treatment planning. Phys Med Biol 1996;41:111-24.

[7] Schneider W, Bortfeld T, Schlegel W. Correlation between CT numbers and tissue parameters needed for Monte Carlo simulations of clinical dose distributions. Phys Med Biol 2000;45:459-78.

[8] Woodard HQ, White DR. The composition of body tissues. Br J Radiol 1986;59:1209-18.

[9] Yang M, Zhu XR, Park PC, Titt U, Mohan R, Virshup G, et al. Comprehensive analysis of proton range uncertainties related to patient stopping-power-ratio estimation using the stoichiometric calibration. Phys Med Biol 2012;57:4095-115.

[10] Saito M. Potential of dual-energy subtraction for converting CT numbers to electron density based on a single linear relationship. Med Phys 2012;39:2021-30.

[11] Tsukihara M, Noto Y, Hayakawa T, Saito M. Conversion of the energy-subtracted CT number to electron density based on a single linear relationship: an experimental verification using a clinical dual-source CT scanner. Phys Med Biol 2013;58:N135-44.

[12] Landry G, Seco J, Gaudreault M, Verhaegen F. Deriving effective atomic numbers from DECT based on a parameterization of the ratio of high and low linear attenuation coefficients. Phys Med Biol 2013;58:6851-66.

[13] Yang M, Virshup G, Clayton J, Zhu XR, Mohan R, Dong L. Theoretical variance analysis of single- and dual-energy computed tomography methods for calculating proton stopping power ratios of biological tissues. Phys Med Biol 2010;55:1343-62.

[14] Hansen DC, Bassler N, Sorensen TS, Seco J. The image quality of ion computed tomography at clinical imaging dose levels. Med Phys 2014;41:111908.

[15] Li T, Liang Z, Singanallur JV, Satogata TJ, Williams DC, Schulte RW. Reconstruction for proton computed tomography by tracing proton trajectories: a Monte Carlo study. Med Phys 2006;33:699-706.

[16] Schulte RW, Bashkirov V, Klock MC, Li T, Wroe AJ, Evseev I, et al. Density resolution of proton computed tomography. Med Phys 2005;32:1035-46.

[17] Hansen MS, Sorensen TS. Gadgetron: an open source framework for medical image reconstruction. Magn Reson Med 2013;69:1768-76.

[18] Agostinelli S, Allison J, Amako K, Apostolakis J, Araujo H, Arce P, et al. Geant4-a Simulation Toolkit. Nucl Instrum Meth A 2003;506:250-303.

[19] Coutrakon G, Hubbard J, Koss P, Sanders E, Panchal M. Beam optics for a scanned proton beam at Loma Linda University Medical Center. Application of Accelerators in Research and Industry 2003;680:1116-20.

[20] Sipala V, Randazzo N, Aiello S, Leonora E, Lo Presti D, Russo M, et al. YAG(Ce) crystal characterization with proton beams. Nucl Instrum Meth A 2011;654:349-53.

[21] Sadrozinski HFW, Johnson RP, Macafee S, Plumb A, Steinberg D, Zatserklyaniy A, et al. Development of a head scanner for proton CT. Nucl Instrum Meth A 2013;699:205-10.

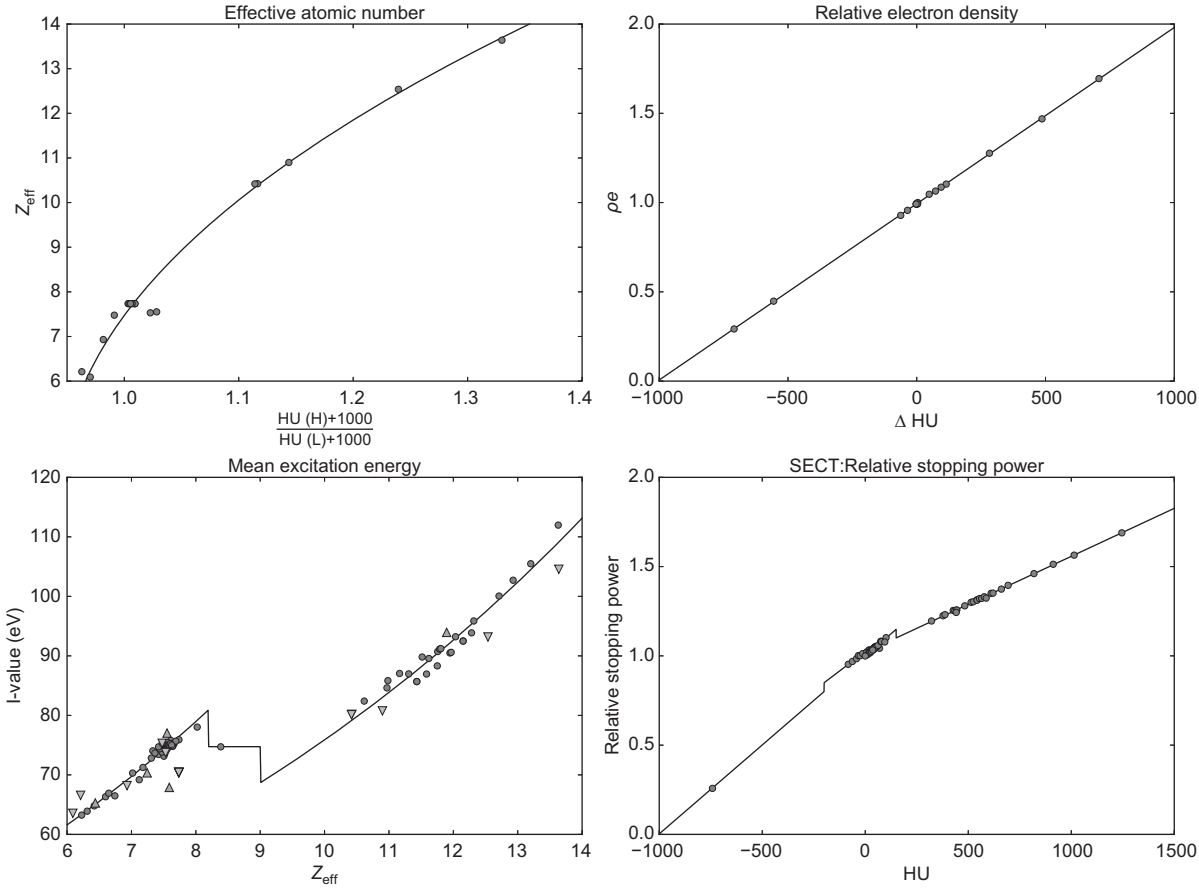

Supplementary Figure 1. Calibration curves for single and dual energy CT. Top left: Ratio between the high and low kVp HU values in the dual energy CT, fitted to effective atomic number, corresponding to the DECT calibration. Top right: ΔHU for the dual energy CT, fitted to electron density, corresponding to the DECT calibration. Bottom left: Effective atomic number fitted to the mean excitation energy (I-value) for tissues from [13]. Upward and downwards triangles indicate the theoretical values for the CIRS and Gammex phantom respectively, added for reference. Bottom right: HU value fitted to relative stopping power via the stoichiometric method for single energy CT, corresponding to the stoichiometric SECT calibration.

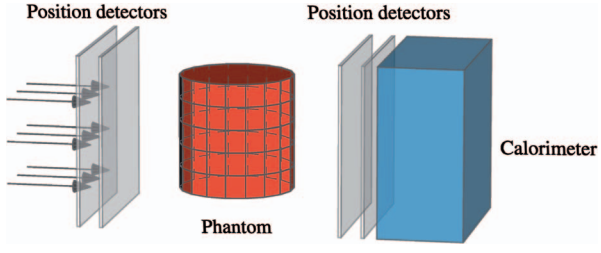

Supplementary Figure 2. Setup of the proton CT simulation, modelled after Sadrozinski et al. [20] and Sipala et al [21].